

## CHAPTER 2. ELECTROCHEMICAL METHODS AND MATERIALS

### 2.1 Electrochemical methods

#### 2.1.1 Controlled-convection technique: rotating ring disc electrode (RRDE)

There are many controlled-convection techniques available but we will restrict our discussion to the two most commonly employed by the electrochemist; the rotating disc electrode (RDE) and the rotating ring disc electrode (RRDE). Until the mid-1940s, most physical electrochemistry was based around the dropping mercury electrode. However, in 1942, V. G. Levich [71] showed that rotating a disc-shaped electrode in a liquid renders it uniformly accessible to diffusion, yet the hydrodynamics of the liquid flow are soluble and the kinetic equations relatively simple. In addition, in contrast to the case of a stationary planar electrode, the current at an RDE rapidly attains a steady state value. However, reversal techniques are not available with the RDE as the products of the electrode reaction are swept from the disc. However, it is possible to intercept solution-borne intermediates or products in their flight away from the disc, by using RRDE, see Figure 2.1.

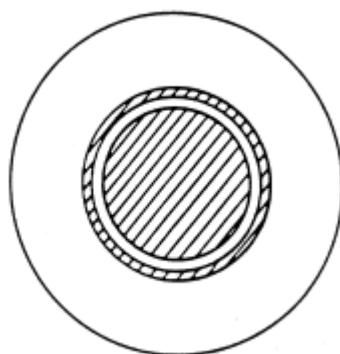


Figure 2.1. Schematic diagram of a ring disc electrode (see text for details).

The disc is held at a potential where the reaction of interest takes place, and an current-potential curve is then recorded at the ring. This allows the identification of intermediates and/or products. A current-potential curve is recorded at the disc while the ring potential is held at a constant value where the intermediates or products are reduced or oxidised. This allows the identification of the exact potential range over which they are formed. Alternatively, the disc is held at a potential where intermediates or products are formed and the ring is maintained at a potential at which they undergo electron transfer. This allows quantitative kinetic measurements to be obtained.

The essentials of RRDE operation are as for the RDE with the addition of one extremely important parameter: the collection efficiency ( $N$ ) could be defined for the reversible reaction:



where  $I_{\text{R}}$  and  $I_{\text{D}}$  are the ring current and disc current, respectively, and the negative sign indicates that the currents are opposed.

If O is reduced at the disc, even if the ring is set at a potential at which the limiting current for the re-oxidation of R occurs, not all of the reduced form produced at the disc will reach the ring surface. For a given system, the fraction of R collected will depend on the geometry of the disc and ring only. The value of  $N$  is given by the Albery-Bruckenstein equation (see [72] for details), though, in practice, for a particular RRDE cell system,  $N$  is determined using a standard redox couple, such as  $\text{Fe}(\text{CN})_6^{4-}$  or  $\text{Br}_2/\text{Br}^-$ . A common value of  $N$  is *ca.* 0.3. The rotation speed provides an independent variable; increasing  $\omega$  decreases the time taken for a species to travel between the disc and the ring and hence increases the likelihood of detecting a short lived intermediate. All of the above methods critically depend on the species generated at the electrode being active towards further electron transfer at the ring.

An informative example of the application of the RRDE concerns the study of the reduction of  $\text{O}_2$  at a Pt disc electrode and the detection of the intermediates and/or products at the Pt ring. The technological importance of oxygen reduction in devices such as fuel cells and metal-air batteries has led to an extensive investigation of the reduction mechanism and particularly of the role of hydrogen peroxide ( $\text{H}_2\text{O}_2$ ) as an intermediate species. Distinguishing between these processes has primarily been

achieved with the rotating ring disc electrode. In  $O_2$ -saturated solutions, a positive potential, high enough to oxidise any  $H_2O_2$  formed at the disc, is applied to the ring and the concentration of  $H_2O_2$  in the solution bulk is kept to a minimum. The potential on the disc is then scanned cathodically and the ring and disc currents simultaneously monitored. A second type of experiment can also be carried out in  $O_2$  free solutions containing  $H_2O_2$ . Now the ring potential is fixed so that all  $O_2$  molecules arriving at the ring are reduced. Thus, any  $O_2$  formed at the disc by disproportionation will be reduced at the ring and a current is seen.

### 2.1.2 Electrochemical impedance spectroscopy (A.C. techniques)

Recently, electrochemical impedance spectroscopy has also been used for the study of the mechanistic origin of electrochemical oscillators such as an active-passive transition of metal surfaces and electrocatalytic oxidation of  $C_1$  fuels.

Methods to excite an electrochemical cell by a sinusoidal signal and the analysis of the currents produced were first employed as a way of measuring the rate constants of fast electron transfer reactions. In any measurement of fast reactions by whatever technique, information has to be obtained at short times, otherwise diffusion rather than kinetics becomes the rate determining process. The A.C. bridge was for a time the only instrumental technique available to allow measurements on the millisecond time scale and below, and the basics of present-day A.C. techniques and methods of analysis were worked out using an electrochemical cell at equilibrium as the unknown arm of a Wheatstone bridge. Modern instrumentation allows A.C. measurements to be made far more expeditiously than with a manually balanced bridge, thus permitting continuous recording of A.C. parameters under dynamic rather than equilibrium conditions, *e.g.*, in cyclic voltammetry or polarographic experiments. At the other end of the time scale, A.C. techniques are now important in corrosion studies, where rapid response is of lesser importance than complete analysis of what are often complicated processes involving surface and solution reactions.

For the study of electrochemical systems, electrochemical impedance spectroscopy (EIS) can give accurate kinetic and mechanistic information with a variety of techniques and output formats. For this reason, EIS is becoming a powerful tool in

the study of corrosion, semiconductors, batteries, electroplating, electro-organic synthesis and electrocatalysis (see Table 2.1).

Research Area	Application
Corrosion	Rate determination, Inhibitor and coatings, Passive layer investigations
Coating Evaluation	Dielectric measurements, Corrosion protection
Batteries/Fuel Cells	State-of-charge, Materials selection, Electrode design
Electrodeposition	Surface pre-treatment, Deposition mechanism
Electro-Organic Synthesis	Adsorption-desorption, Reaction mechanism
Semiconductors	Photovoltaic work

Table 2.1. Summary of some of the electrochemical phenomena that have been studied using EIS.

### Advantages of EIS techniques

**Small amplitude:** EIS techniques use very small excitation amplitudes, often in the range of 5–10 mV peak to peak. Excitation waveforms of this amplitude cause only minimal perturbation of the electrochemical test system, reducing errors caused by the measurement technique.

**Mechanism study:** Since electrochemical impedance experiments provide data on both electrode capacitance and charge-transfer kinetics, EIS techniques can provide valuable mechanistic information.

Measurement accuracy: Since the method does not involve a potential scan, one can make measurements in low conductivity solutions where D.C. techniques are subject to serious potential-control errors. In fact, one can use EIS to determine the uncompensated resistance of an electrochemical cell.

Theoretical advantages: The main advantage of EIS is that one can use a purely electronic model to represent an electrochemical cell. An electrode interface undergoing an electrochemical reaction is typically analogous to an electronic circuit consisting of a specific combination of resistors and capacitors. One can take advantage of this analogy by using an established A. C. circuit theory to characterise the electrochemical system in terms of its equivalent circuit.

In practice, an impedance plot obtained for a given electrochemical system can be modelled with one or more equivalent circuits. This information can be used to verify a mechanistic origin of the system, or at least to rule out incorrect models. Once a particular model is chosen, one can correlate physical or chemical properties with circuit elements and extract numerical values by filtering the data to the circuit model.

### 2.1.3 Auger electron spectroscopy (AES)

If a vacancy is created in an atomic core level, for example, by irradiation with X-rays, as above, or with electrons, then an electron from an upper level can be expected to fill the hole. Figure 2.2 is a schematic view of the process in which a K-shell vacancy in silicon is filled by an  $L_1$  electron. The energy difference liberated by this relaxation is 1690 eV, and it can be entirely released in the form of a photon (X-ray fluorescence) by ejecting an Auger electron from the atom. In the example of Figure 2.2, the Auger electron comes from the  $L_{2,3}$  shell. The required energy loss of 1690 eV is divided into the energy required to remove the electron from the sample (mostly its binding energy) and the kinetic energy it retains upon entering the vacuum. Since the total energy of the transition and the binding energy are well-defined values, the kinetic energy of the Auger electron *in vacuo* is also well-defined. By measuring the distribution of electrons vs. kinetic energy, one can obtain a spectrum showing sharp

peaks at the discrete Auger energies. Each Auger line is characteristic of the originating atom and can be used analytically to indicate the presence of that species.

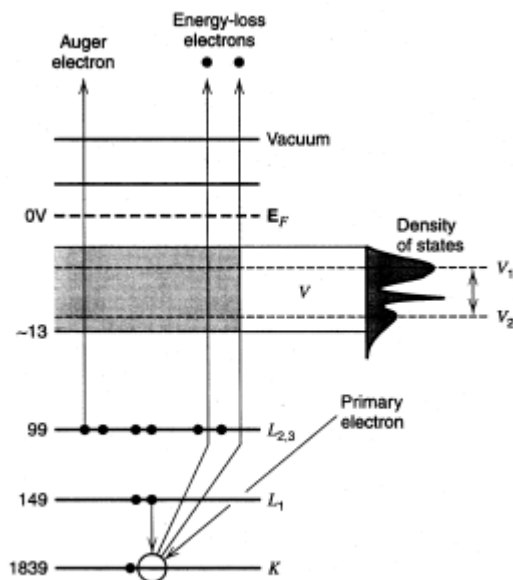


Figure 2.2. Schematic view of the Auger emission process from silicon. The atom is ionised initially by an incident electron. That electron and one from the K-shell leave the sample as energy loss electrons. The energies of the levels relative to the Fermi level,  $E_F$ , are given on the left.

Auger transitions are conventionally labelled with a three letter notation indicating the shell of the primary vacancy, the shell of the filling electron, and the shell from which the Auger electron was emitted. Thus, the transition in Figure 2.2 is called the  $KL_1L_2$  or  $KL_1L_3$  process. Any given atom may show several Auger transitions, hence several lines in the spectrum.

If the electron is scattered inelastically during its passage through the sample, its kinetic energy *in vacuo* will differ from the characteristic Auger energy, and it will contribute only to the broad continuum on which the Auger lines are superimposed. Thus, Auger electron spectrometry (AES) is strictly a surface technique, in which atoms only within about 20 Å from the surface can contribute unscattered electrons.

In most instruments, an electron beam, which can be focused to a smaller spot size than an X-ray beam, is used to excite the sample. The spectrum of emitted and scattered electrons, including Auger electrons, is analysed according to the kinetic

energy in a manner that produces a derivative readout, so that the sharp Auger structure is more easily seen on the broad continuum.

### 2.1.4 Low-energy electron diffraction (LEED)

Electrons travelling *in vacuo* at kinetic energies in the range from 10 eV to 500 eV have de Broglie wavelengths on the order of angstroms; hence one could expect a monochromatic beam of these electrons to be reflected from an ordered solid in a diffraction pattern that provides information about the structure of the solid. This effect is the basis of low-energy electron diffraction (LEED).

A LEED experiment differs significantly from other types of diffraction experiments, in that the probing beam cannot penetrate the sample to a distance greater than a few angstroms without being scattered inelastically and losing energy. Thus, it is unable to sampling the three-dimensional order of the solid, and any observed diffraction is due to the two-dimensional order of the surface. Thus, LEED is a very specific tool for examining the geometric patterns of atoms on a surface, and it has been widely used for studies of adsorption from the gas phase and catalysis of gas-phase/solid surface reactions. LEED is also employed to characterise electron surfaces, especially single-crystal electrons that produce well-defined diffraction patterns [73, 74].

Figure 2.3 is a schematic diagram of a typical apparatus. The chamber is always at ultra high vacuum ( $< 1 \times 10^{-8}$  mbar), so that the surface remains clean during the experiment. Electrons are directed toward the sample in a beam and are reflected diffractively along certain well-defined lines. The grids filter out inelastically scattered electrons (at low energy) and then allow the diffracted ones to accelerate toward a luminescent screen. Bright spots on the screen can be observed and photographed from the viewing port. The arrangement of this system also allows AES experiments to be done by changing the signals on the grids and the energy of the electron beam. One very frequently finds combined LEED/Auger systems in use, because it is convenient to be able to monitor surface contamination or adsorption by AES during LEED studies.

Different spot patterns can be interpreted in terms of different surface structures in a fairly straightforward manner. There is a standard notation for describing the structures and their corresponding patterns, but it is beyond our scope to delve into it

here. In electrochemical experiments, LEED is used to define the structure of a single-crystal electrode surface [e.g., the (100) face of Pt] before its use in a cell, and to monitor changes that may have taken place upon immersion or electrochemical treatment.

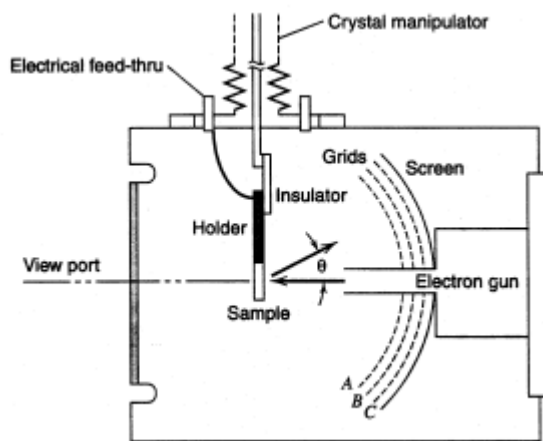


Figure 2.3. Schematic diagram of a LEED apparatus [75].

### 2.1.5 Reflection high-energy electron diffraction (RHEED)

If a beam of high-energy electrons is incident upon a flat surface in grazing incidence (see Figure 2.4), the diffraction pattern formed will be characteristic of the surface atomic arrangement because the component of the incident electron momentum normal to the surface is very small and, thus, the penetration of the electron beam will be small. At high energies, the wavelength of the electron is small and the radius of the Ewald sphere is large compared with typical reciprocal lattice vectors. Thus, at 100 keV,  $\lambda = 0.0037 \text{ nm}$  and  $|k_0| = 1700 \text{ nm}^{-1}$ , whereas  $2\pi/a$  might typically be  $20 \text{ nm}^{-1}$ . Compared with the reciprocal lattice, the Ewald sphere is very large and will cut the (00) rod almost along its length, as indicated in Figure 2.4(b). Only those rods in the plane normal to the paper and containing the (00) rod will contribute beams to the diffraction pattern. This RHEED pattern will therefore consist of long streaks normal to the shadow edge of the sample and spaced by a distance  $t$ . If the separation between the fluorescent screen and the sample of some cubic crystal is  $L$  (the camera length) and the distance between streaks on the screen is  $t$ , then

$$t = L \tan 2\theta, \quad (2.2)$$

by geometry and

$$\lambda = 2d \sin\theta = \frac{2a}{(h^2 + k^2)^{1/2}} \sin \theta, \quad (2.3)$$

by Bragg's law for a sample with a square lattice of side  $a$ . As  $\lambda \ll a$  in RHEED, then the value of  $2\theta$  is small and these equations can be simplified to yield

$$a = (h^2 + k^2)^{1/2} \lambda L/t. \quad (2.4)$$

All the parameters on the right-hand side of Eq. (2.4) can be deduced or measured and, thus,  $a$  can be determined. The accuracy with which this can be done is determined largely by accuracy with which  $t$  can be measured. This is determined largely by the length  $L$ . High-accuracy RHEED experiments are usually constructed so as to have long camera lengths for this reason.

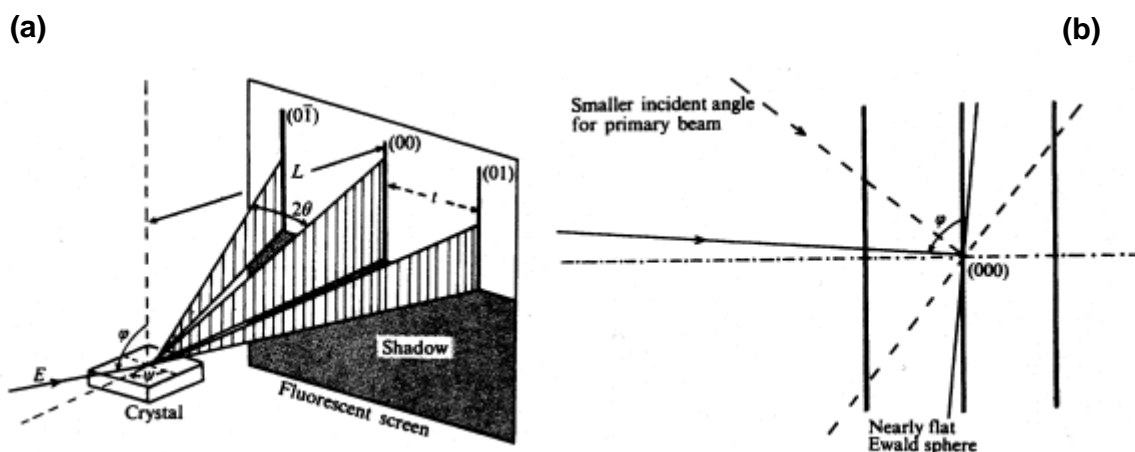


Figure 2.4. The RHEED method. (a) Experimental geometry. A fine parallel beam of electrons is incident near  $\phi = 90^\circ$  upon a flat single-crystal surface. (b) Ewald sphere construction for RHEED.

Since the Ewald sphere is so large in a RHEED experiment, it is necessary to change the diffraction geometry in order to find an arrangement of reciprocal lattice rods in three dimensions and, thus, to define the unit mesh. As can be seen using Figure 2.4(b), all the reciprocal lattice rods can be explored either by changing the angle  $\phi$  by rocking the sample about an axis in its surface or by rotating the sample about its surface normal. The latter is to be preferred if constant surface sensitivity is to be maintained, as the rocking experiment changes the component of the incident electron momentum normal to the surface. If the azimuthal angle is varied, sample streak diffraction patterns can be observed when the incident beam is along the direction of high crystal symmetry.

### 2.1.6 Interfacial potential measurements

The monitoring of local electrical potential by using *in-situ* potential microprobes is a technique which allows to measure the spatial potential distribution. Experiments in which spatiotemporal visualisation of interfacial potential distribution along the electrified interface between solid electrode and the electrolyte is of special interest have been performed many times. In the early 1950s, Franck [7] studied activation front patterns in one-dimensional space with three stationary probes, and Lev *et al.* [12] used 15 microelectrodes to obtain the space-time pattern in the anodic dissolution of nickel (Ni). Recently, Flätgen [19, 76] measured one-dimensional images on a rotating ring electrode with a single stationary potential microprobe placed near the ring electrode. On the other hand, two-dimensional observations with potential microprobes have been a challenging task and, thus, have only been investigated in a few systems such as metal corrosion [77, 78].

Two basic types of potential microprobes have been described. One is based on potentiometric probing and it consists of a reference electrode, *e.g.*, Hg/Hg<sub>2</sub>SO<sub>4</sub> or Ag/AgCl, mounted in a small glass capillary. These potential microprobes were usually applied for the measurement of potential distributions. The current flowing through the capillaries is negligible. The other one is a thin metal wire (*e.g.*, Pt), which is sealed into a glass tube except for the tip. It might measure the mass-transport, diffusion coefficient and interfacial kinetics. The setup used for a ring electrode in the present work consisted of 11 (or 12) equally spaced identical Hg/Hg<sub>2</sub>SO<sub>4</sub> electrodes as illustrated in Figure 2.5.

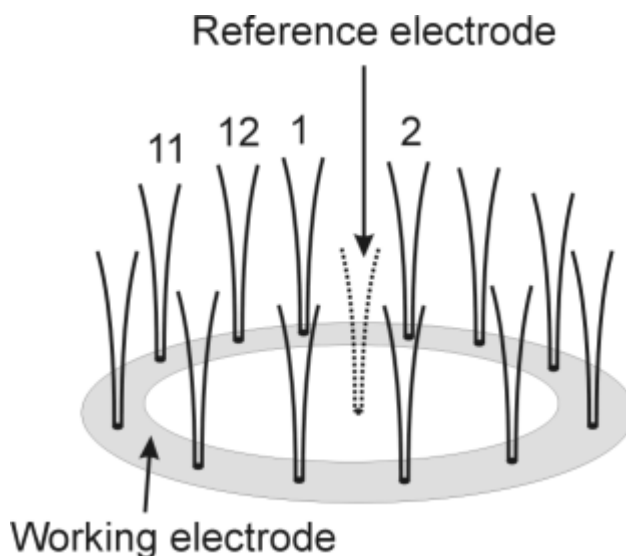


Figure 2.5. Side view of the multi-electrode array setup for the measurements of spatial potential distribution along a ring working electrode (counter electrode not shown).

These capillary probes were used in order to understand the spatiotemporal pattern of the interfacial potential associated with the oxidation of formic acid (HCOOH) on Pt ring and ribbon-shaped electrodes. The details of the experimental setup on Pt ring and ribbon to monitor the spatiotemporal data will be demonstrated in section 4.4.1 and 5.2.1, respectively.

### **Resolution of spatiotemporal fine structure (extrapolate)**

The temporal resolution of the multi-probe setup is either given by the characteristic time scale  $\tau$  of the potential probes or by the reciprocal value of the sampling frequency ( $f_{\text{sample}}$ ) of the ADC. The value of  $f_{\text{sample}}$  is given by the hardware and software configuration of the data acquisition setup. In order to minimise  $\tau$ , the conductivity  $\sigma$  of the solution inside the capillary has to be maximised, for the capillary constitutes an electrical parallel RC circuit composed of the capillary's capacity and its solution resistance. For a typical value of the capillary capacity ( $10^{-8}$  F) and  $\sigma$  of the solutions employed,  $\tau$  can be estimated to range from 0.1 – 10  $\mu\text{s}$ , which proved to be sufficient for the temporal processes considered. The spatial resolution follows primarily from the spacing of the local probes along the electrode. Furthermore, the

measured local potential value depends also on the individual distance of the probe from the working electrode surface, since the distance determines the width of the spatial region over which an averaging of the potential occurs.

Due to the strong migration coupling, the expected characteristic spatial length scale of electrochemical patterns is large compared with reaction-diffusion systems. Thus, the given basic spatial resolution of about 10 mm was assumed to be sufficient to record the spatial potential inhomogeneities.

## 2.2 Materials and solutions

### 2.2.1 Three-electrodes used

#### Working electrode

Designs of working electrodes are diverse. Most commonly in experiments to study mechanism and kinetics in the laboratory, the working electrode is a small sphere, disc, or a short wire, but it could also be metal foil, a single crystal of metal, an evaporated thin film, or a powder in the form of pressed disc or pellets. An essential feature is that the electrode should not react chemically with the solvent or solution components. The useful working range is difficult to define as it may be limited by a number of different processes such as oxide formation, hydrogen or oxygen evolution, or solvent decomposition, as well as depending on the reactants and products of the system under study. It is desirable to have an even current and potential distribution and hence for the cell to be designed, so that all points on the working electrode surface are geometrically equivalent with respect to the secondary electrode.

Single crystal Ru electrode: In Chapter 3, a Ru (0001) single crystal prepared by the Crystal Laboratory of the Fritz-Haber-Institut was employed as working electrode. It was oriented within 0.5 °. The geometric area of the Ru (0001) single crystal disc with a diameter of 7 mm (thickness of 2 mm) is 0.385 cm<sup>2</sup>.

Pt Ring- and ribbon-shaped electrode: In Chapters 4– 6, polycrystalline Pt electrode (MaTeck, 99.99 %, thickness of 0.1 mm) were used to investigate the different spatiotemporal pattern formations of interfacial potentials in different geometries.

### **Counter electrode**

The purpose of the counter electrode is to supply the current required by the working electrode without limiting the measured response of the cell. It is essential that the electrode process is a decomposition of the electrolyte medium or the oxidation/reduction of a component of the electrolyte, so that the current flows readily without the need for a large overpotential. In some cases, it can be arranged that the counter electrode reaction is a gas evolution or the reverse of the working electrode reaction, so that the composition of the electrolyte is unaltered. The products of the counter electrode reaction should always be considered since they must not interfere with the reaction being studied on the working electrode. This is a particularly difficult problem in aprotic media where the counter electrode reaction invariably leads to the decomposition of the solvent and a complex mixture of species in the solution; at least, the decomposition of water causes only gas evolution and maybe a pH change. In practice, such interference is perhaps best minimised by isolating the anolyte and catholyte with a frit or an ion exchange membrane. Ionic conduction is maintained, but the mixing of the respective solutions is prevented. An alternative approach is to seek an electrode reaction which leads only to non-contaminating products, *e.g.*, an insoluble solid on the electrode surface or an innocuous metal ion solution. As noted above, the counter electrode should not impose any characteristics on the measured data and, in consequence, it should have a large area compared with the working electrode. Moreover, as also noted above, its shape and position are important since these determine whether the working electrode is an equipotential surface, and consequently, it is preferable to avoid a separator in the cell. This requires the choice of clean counter electrode chemistry.

Platinized Pt cathode: A platinized Pt electrode was used in this work, except in Chapter 3. The preparation of the electrode is as follows. First, a thin wire with thickness of 1 mm is chemically cleaned in  $\text{H}_2\text{Cr}_2\text{O}_4/\text{H}_2\text{SO}_4$  or  $\text{H}_2\text{SO}_4/\text{H}_2\text{O}_2$  (or  $\text{HNO}_3$ ) for 1 min and it is boiled in conc. HCl for 1 min, followed by rinsing with ultrapure water. Then, black

Pt can be cathodically deposited in 1 %  $\text{H}_2\text{PtCl}_6/0.5 \text{ M HCl}$  at the  $\text{H}_2$  evolution potential (or current) for 5 min. After rinsing of the electrode with ultrapure water, one can anodically make a rougher electrode to increase the real surface area at  $\text{O}_2$  evolution for 3 min in the same solution. Finally, the platinized Pt electrode is completely cleaned in ultrapure water. In Chapter 3, a Pt wire was used as CE.

### Reference electrode

The role of the reference electrode (RE) is to provide a fixed potential which does not vary during the experiments (*e.g.*, it should be independent of current density). In most cases, it will be necessary to relate the potential of RE to other scales, for example to the normal hydrogen electrode, the agreed standard for thermodynamic calculations. In potentiostatic experiments the potential between WE and RE is controlled by a potentiostat, and as the reference half cell is maintained at a fixed potential, any change in applied potential to the cell appears directly across the interface between WE and solution. The RE serves dual purposes of providing a thermodynamic reference and also isolating WE as the system. In practice, however, any measuring device must draw a current to perform the measurement. Thus, a good RE should be able to maintain a constant potential even if a few microamperes are passed through its surface. This criterion will be satisfied if the exchange current density is high and hence, the reaction is totally reversible.

In Chapters 4– 6, the  $\text{Hg/Hg}_2\text{SO}_4$ , saturated  $\text{K}_2\text{SO}_4$  (+ 640 mV *vs.* NHE) was used as a reference electrode, since it is a useful electrode for sulphate solutions but becomes unstable if the sulphate concentration falls below 0.1 M. On the other hand, during electrochemical experiments in Chapter 3 connected with the ultra high vacuum chamber (RHEED and LEED apparatus), a  $\text{Ag/AgCl}$  electrode in saturated KCl solution (+ 197 mV *vs.* NHE) was used in order to avoid the consideration of the adsorption effect of sulphate ions on the substrate.

### 2.2.2 Electrolytes

The electrolyte is the medium between the electrodes in the cell, and it consists of the solvent and a high concentration of an ionised salt as well as the electroactive

species. It may also contain other materials, complexing agents, buffers, etc. The supporting electrolyte is present (a) to increase the conductivity of the solution, hence, to reduce the resistance between WE and CE, (b) to minimise the potential error due to the uncompensated solution resistance ( $R_u$ ), (c) to minimise the variation of  $\phi_2$ , the outer Helmholtz plane potential, with applied potential and thereby to suppress the double layer effect on kinetics and (d) to effectively eliminate migration as a mode of mass-transport for the electroactive species. Electrode reactions can be extremely sensitive to impurities in the solution; for example, organic species are often strongly adsorbed even at  $1 \times 10^{-4}$  mol/L bulk concentration from aqueous solutions. Hence, salts should be of the highest available purity and/or recrystallised, the solvent should be carefully purified, and the solutions must be carefully deoxygenated.

All solutions used in this thesis were prepared using triply distilled deionised water (Millipore, 18.2 M $\Omega$  cm). Prior to all experiments, solutions were purged with high-purity nitrogen (99.999 %, Linde Technische Gase) in order to remove dissolved oxygen. In many experiments, the cell was kept under a nitrogen atmosphere during experiments to avoid the diffusion of air oxygen into the solution. Details on chemicals, purity, and concentrations of electrolytes will be explained in the each experimental section of the forthcoming chapters.

### 2.2.3 Reaction modifiers

Effects of surface modification to enhance the electrocatalytic activity should be briefly explained, since Bi modification was done in Chapters 4 and 5, and ruthenium modification in Chapter 6 to improve the electrocatalytic activity of the Pt working electrode. The tendency of both formic acid and methanol reactions to self-poison makes clear that catalyst properties must be changed to avert the poisoning conditions. As in many other catalytic systems, manipulation of the composition of the catalyst may allow for the modification of reactivity.

The roles of reaction modifiers have been discussed in several studies [79 – 81]. The principal functions of modifiers are to decrease the poisoning branch in the reaction and to increase the direct oxidation rate. Modifiers may perform their roles by the following four mechanisms: (i) third-body effect, (ii) bifunctional theory, (iii) electronic

modification and (iv) destabilisation of the poison. To begin with, the third-body mechanism refers to the interruption of large ensembles of substrate atoms by a modifier. Especially, HCOOH oxidation on Pt occurs through a dual path mechanism shown in Figure 2.6, in which one path goes through an active intermediate (most likely COOH) and the other through a poison intermediate (CO).

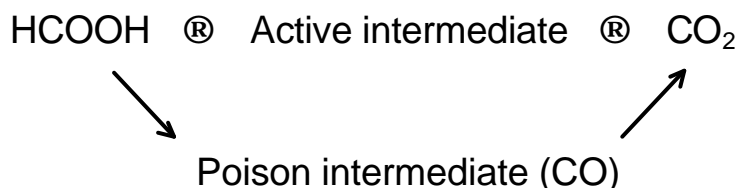


Figure 2.6. Dual path mechanism of HCOOH oxidation on a Pt electrode.

For example, in the third-body theory, the inactive intermediate species (CO) requires a minimum number of adjacent free sites of Pt to form on the surface. If the Pt substrate is modified by the adsorption of Bi ions, the Bi modifier blocks the adsorption of CO, so that HCOOH is directly oxidised to CO<sub>2</sub>. A third-body effect is a steric effect. Secondly, the bi-functional mechanism is relating to catalysts on which the different components have separate and distinct roles in the oxidation reaction of small organic molecules (C<sub>1</sub>). For instance, in the oxidation of methanol or formic acid on 50 % Ru/50 % Pt alloy, 10 % Ru/90 % Pt and Bi deposition on Pt, Pt atoms dissociate fuels into intermediate species and Ru or Bi adsorb oxygen containing species. Both Pt and foreign catalytic materials are necessary for complete oxidation, CO<sub>2</sub> evolution. Finally, the electronic effect of a modifier is explained by the interaction of reactant substrates. In the Bi-modified Pt (111) single crystal, Bi ad-atoms alter the electronic interaction of adsorption species and substrate. Thus, the saturation coverage of the poison species, CO, was drastically decreased in the presence of an extremely small coverage of Bi on the Pt substrate by electrochemical deposition.

## 2.3 Instruments and data processing

### 2.3.1 Instruments

#### Potentiostat

The potentiostat is a device for controlling the potential between RE and WE at a fixed and selected potential. The simplest setup, which is of little practical use but outlines the principle, is shown in Figure 2.7 where the cell has been approximated by a very simple equivalent circuit of a solution resistance in series with a double layer capacitance. It can be seen that the device is simply a voltage follower maintaining the output voltage between RE and WE at the programming potential  $E_1$ . WE has a potential  $-E_1$  relative to RE, so that the input voltage is inverted in the cell. Also in this arrangement there is no device for measuring the current through the cell and the potentiostat is unable to apply more than a single potential at any one time.

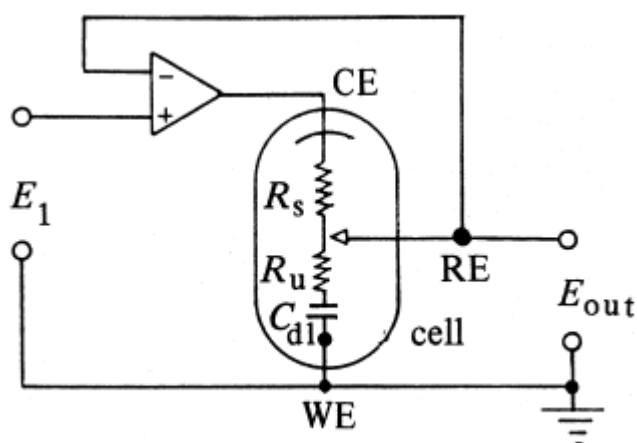


Figure 2.7. Simple potentiostat for maintaining a constant potential between a reference electrode (RE) and a working electrode (WE);  $R_s$  is the solution resistance between the RE probe and the counter electrode (CE);  $R_u$  the uncompensated resistance between the Luggin tip and WE; and  $C_{dl}$  the double layer capacitance of the working electrode.

In this thesis mostly a potentiostat provided by the Electronic Laboratory of Fritz-Haber-Institut was used. The circuit is based on the idea of D. Roe [82]. A bipotentiostat/galvanostat (EG&G model 366) served as power source for the ring disc measurements and galvanostatic scans (Chapters 4 and 6).

### Galvanostats

The simplest way to obtain a constant current is to apply a voltage from low output impedance voltage sources across a large resistor in series with the cell, as shown in Figure 2.8. The current will be given by the ratio  $E_m/R$  (the provided resistance  $R$  is very large compared with the impedance of the cell).

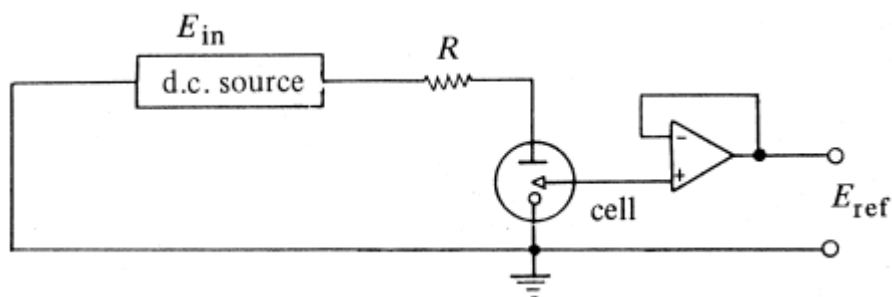


Figure 2.8. Early galvanostat circuit.

Several operational amplifier circuits are also available for galvanostats. Two of the simplest are shown in Figure 2.9. The circuit arrangement is that of the voltage follower with the cell in the feedback loop, and the current is again determined by the ratio  $E_m/R$ . The configuration in Figure 2.9(a) has the advantage that WE is at virtual ground. Thus, the reference potential,  $E_{ref}$ , can be monitored using a voltage follower. However, the output impedance of the voltage source,  $E_m$ , must be able to supply the required current into the feedback loop. In the configuration of Figure 2.9(b) the current is supplied by the output of the operational amplifier, but the working electrode is not at virtual ground, so that  $E_{ref}$  has to be monitored with a differential voltmeter. Most potentiostats can be converted to a galvanostat by inserting a standard resistor  $R$

between working and reference inputs of the instrument and then by connecting WE to RE input and CE in the normal configuration.

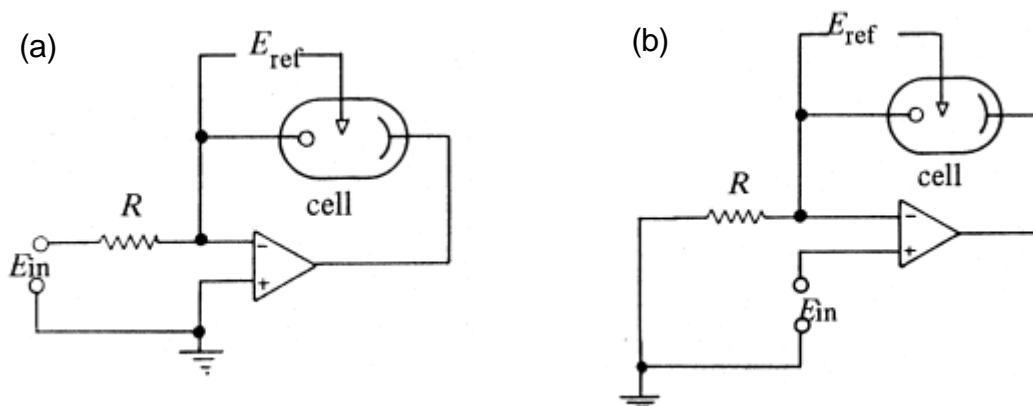


Figure 2.9. Two galvanostat circuits employing operational amplifiers.

### 2.3.2 Data acquisition and processing

In Figure 2.10 the principal elements involved in the complete experimental cell and data acquisition setup are sketched. The pulse perturbation electrode is connected to the 20 MHz Pulse Generator (HM 8035, ELAB of FHI) providing rectangular potential pulses (DC mode) of various duration and amplitude. Without external resistance, amplitudes of the potential pulses are relative to the working electrode potential. WE, CE and RE are connected to the potentiostat/galvanostat, which also controls an X–Y recorder (KIPP & ZONEN). The local potential probes are connected through a combined low-pass filter/floating-ground amplifier ( $\times 10$ , ELAB of FHI) (circuit is shown in Figure 2.11) to the input channels of a 12 Slot VME-bus-16 channel multiplex analogue digital converter (ADC). During measurements, digital information is temporarily stored in the data acquisition device before being passed on to a permanent storage (IBM compatible PC) after completion of measurements.

The JAVA measurement software written by H. Junkes and S. Schöne at the computational centre of the Fritz-Haber-Institut is executed from the PC by clicking on START/Programme/Java Messprogramm/**Soundgarden** measurements controlled by a

mouse. After a window pop-up, the software needs to be connected to the acquisition device (CPU with a DNS entry link) by pressing **CONNECT**. The software is now by default set in the on-line, **STAND-BY** mode, *i.e.*, a mode without storing information, but instead where the instantaneous potential information can be inspected in a time series and a (potential-channel) plot representation. Upon starting the acquisition mode (**START** button), the instantaneous graphs are deactivated. Instead, the 16 channels information is read into the temporary memory and is transferred to the PC's hard disk after termination (**STOP** button). Apart from a setup information ASCII file including the information provided by the user in the lower window, an ASCII text file is created with 16 columns and the number of rows equalling the number of multiplexed input cycles. Being ASCII, the information is easily retrievable. The scanning frequency is variable between 40 Hz and 1000 Hz.

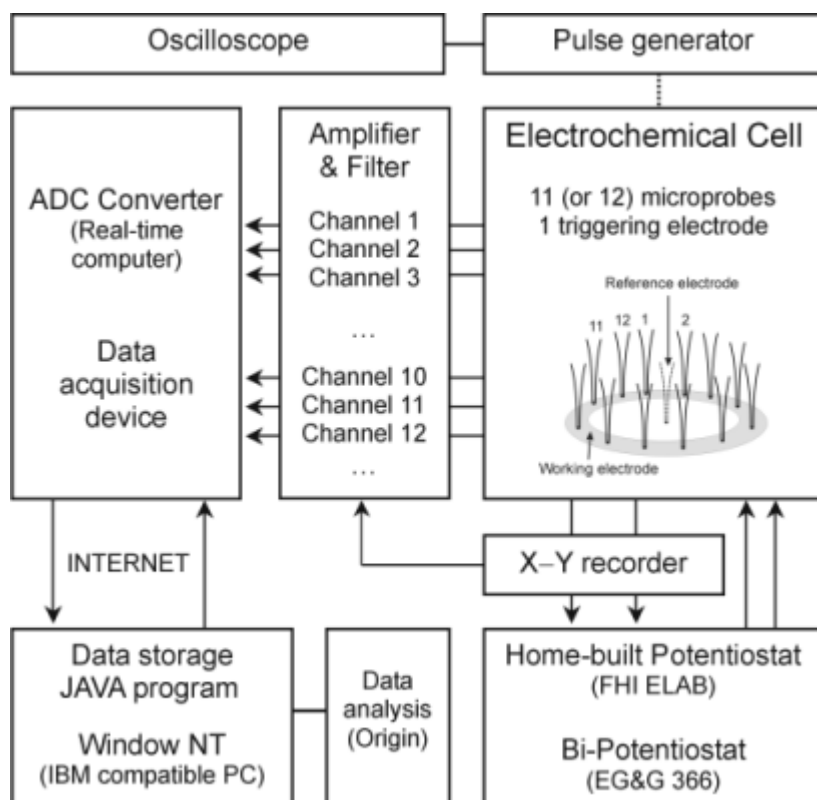


Figure 2.10. The sketch of principal experimental setup for the data acquisition during multi-potential probe measurements.

As the A/D multiplex converter is of 12 bit resolution within a voltage range of  $\pm 10$  V, a maximal signal resolution of about 5 mV could be achieved in the local potential measurements. This potential resolution was considered to be quite sufficient, as potential variations due to dynamical instabilities were expected to be on the order of several hundred mV (see experimental section of ref. [83] for a better understanding).

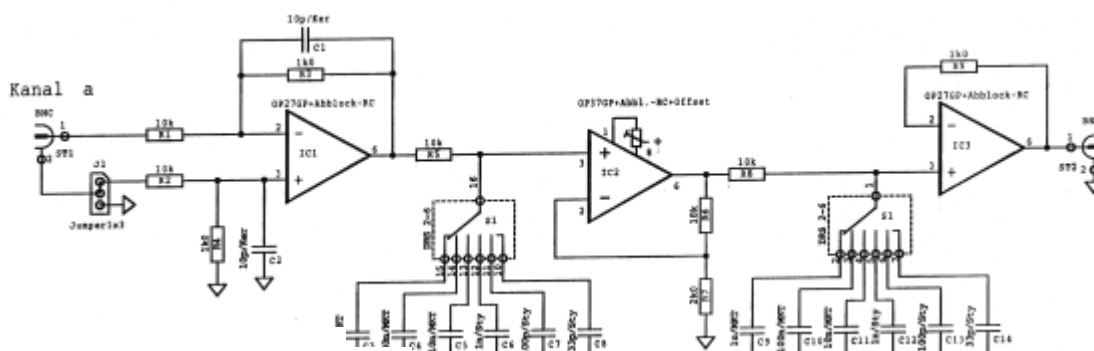


Figure 2.11. Electronic circuit of the amplifier and filter with floating ground used for the spatially resolved measurements of the local potential drop at the electrode surface. Adapted from Electronic Lab (**ELAB**) of Fritz-Haber-Institut.

Apart from inherent measurement noise, systematic errors occurred due to the following reasons: (i) the small inner diameter of the local capillary potential probes, (ii) the ohmic potential drop across the electrolyte due to spatial inhomogeneities of the conductivity of the electrolyte (*i.e.*, leakage of the capillary solution) and different distances between the tip end of the capillary and the surface of working electrode.

While the variations of the inner diameter mainly affected the characteristic time scale of the capillaries and, therefore, did not considerably influence the magnitude of the measured local potential, variations of the solution conductivity inflicted the measured local potential, in particular at high ( $\geq +0.5$  V) and very low ( $\leq -0.5$  V) overpotentials. At potentials considered under bistable and oscillatory conditions, the maximal system error of individual potential probes observed in experiments never exceeded 10 % (with respect to the average of the remaining ten electrodes).

Since all local potential probes are stationary, data processing is straightforward. Where a systematic error occurred, a linear normalisation was performed which allowed for the elimination of the systematic potential error. All figures in the upcoming

experimental chapter were plotted by means of using Origin professional 6.0 (Microcal Software, Inc.) and all figures result from the original raw data without any subsequent digital filtering and processing. Detailed data processing in Origin is as follows.

- Import the raw data (ASC II): Import → Single ASC II → R:\measurements\\*.txt
- Convert raw data into the matrix: Edit → Convert to Matrix → Direct
- Make sure the property of matrix: Matrix → Set Dimensions
- Plot figures: Plot 3D → 3D Color Fill Surface (or Contour-Color Fill)
- Adjust colour map and contours: Format → Plot
- Adjust size and speed: Format → Layer.